sind die als WELKERsche Regel bekannt gewordenen Gesetzmäßigkeiten [13] und der von GUTBIER gefundene Zusammenhang zwischen der Breite der verbotenen Zone und dem partiellen Ionencharakter der Bindung bei Tetraederstruktur [14]. Bei unregelmäßiger Anordnung von gleichen Atomen, wie z. B. in atomaren Schmelzen, trifft die linke Hälfte der Abb. 1 zu, in der keine Energielücke vorhanden ist. Daher gehen halbleitende Elemente in metallisch leitende Schmelzen über.

Die einfache Abhängigkeit des Ionencharakters einer Verbindung von der Atom- und Elektronendichte sowie von atomaren Größen läßt noch eine thermodynamische Deutung des Bindungszustandes zu. Vergleicht man nämlich den Exponentialansatz (1) für die Wahrscheinlichkeiten mit dem BOLTZMANN-Faktor, dann entspricht der Größe β^{-1} gerade die thermische Energie RT (R = Gaskonstante) eines Mols von BOLTZMANN-Teilchen. Bei vorgegebenem β^{-1} im Festkörper bzw. RT im BOLTZMANN-Gas ist damit die Verteilung des Systems auf die einzelnen Energieniveaus bestimmt. Da diese Verteilung dem Zustand maximaler Entropie entspricht, läßt sich der Bindungszustand, wenigstens formal, wie folgt beschreiben: Bei konstanter Dichte (und damit konstantem Volumen) ist die als innere Energie auftretende Austauschenergie β^{-1} ebenfalls konstant. Von allen hiermit verträglichen Bindungszuständen ist dann derjenige realisiert, für den die Entropie ein Maximum wird.

Ich danke den Herren Dr. GUTBIER und Dr. LÜTGEMEIER für zahlreiche wertvolle Diskussionen und Frl. DICK für ihre sorgfältige Mithilfe bei der numerischen Rechenarbeit.

[13] H. WELKER, Z. Naturforschg. **7 a**, 744 [1952].

[14] H. GUTBIER, Vortrag auf der Tagung des Fachausschusses Halbleiter, München, April 1964.

Dynamical Theory of Electron Diffraction for Finite Crystals

FUMINORI FUJIMOTO *

Fritz-Haber-Institut der Max-Planck-Gesellschaft, Berlin-Dahlem **

(Z. Naturforschg. **20 a**, 367—379 [1965]; eingegangen am 3. Oktober 1964)

The dynamical theory of electron diffraction for a finite crystal is developed by using higher BORN approximations. The general formula obtained here is applied to wedge-shaped and spherical crystals. In the latter case, the intensity, integrated intensity and line breadth of the DEBYE–SCHERRER ring are calculated. The results indicate an anomaly of line breadth.

The intensity of DEBYE–SCHERRER rings in electron diffraction has recently been studied by many workers and the results have been compared with the theory. The theoretical treatments have been, however, based on the assumption of an infinite parallel-sided crystal. This assumption is usually not adequate to the experimental conditions.

KATO [1] has extended the dynamical theory to the case of a finite polyhedral crystal using the boundary conditions of KIRCHHOFF. According to his result, the wave function of the transmitted electron is represented by the product of the diffraction functions of the entrance and exit surface and the wave function obtained from the usual dynamical theory.

On the other hand, the BORN approximation has recently been developed by FENGLER [2] for the case of a finite crystal. He has calculated exactly the second order approximation for a spherical crystal and compared the result with that for a parallel-sided crystal.

In the present paper, we intend to develope FENGLER's theory and to apply it to the LAUE-case for wedge-shaped and spherical crystal form. In the latter case, moreover, we calculate the intensity, integrated intensity, and line breadth of the DEBYE–SCHERRER ring.

* On leave from the University of Tokyo, College of General Education, Tokyo, Japan.

** Abteilung Prof. Dr. K. MOLIÈRE.

[1] N. KATO, J. Phys. Soc. Japan **7**, 397, 406 [1952].

[2] H. FENGLER, Z. Naturforschg. **16 a**, 1205 [1961].

§ 1. Fengler's Theory [2]

The wave function of the scattered electron, $\psi(\boldsymbol{r})$, should satisfy the integral equation

$$\psi(\boldsymbol{r}) = \exp(i\,\boldsymbol{K}_0\,\boldsymbol{r}) + \frac{2\,m}{\hbar^2}\int G(\boldsymbol{r},\boldsymbol{r}')\,V(\boldsymbol{r}')\,\psi(\boldsymbol{r}')\,\mathrm{d}(\boldsymbol{r}')\,, \tag{1}$$

where $\boldsymbol{K}_0$ is the wave vector of the incident electron in the vacuum and $V(\boldsymbol{r})$ is the potential energy. GREEN's function, $G(\boldsymbol{r},\boldsymbol{r}')$, is given by

$$G(\boldsymbol{r},\boldsymbol{r}') = \lim_{\varepsilon\to+0}\frac{1}{(2\,\pi)^3}\int\frac{\exp[i\,\boldsymbol{k}\,(\boldsymbol{r}-\boldsymbol{r}')]}{K_0{}^2-k^2+i\,\varepsilon}\,\mathrm{d}(\boldsymbol{k}) = -\frac{1}{4\,\pi}\frac{\exp[i\,K_0\,|\boldsymbol{r}-\boldsymbol{r}'|]}{|\boldsymbol{r}-\boldsymbol{r}'|}\,. \tag{2}$$

The other notations have their usual meaning. When the crystal is finite, the potential energy of the electron can be represented by

$$-\frac{2\,m}{\hbar^2}V(\boldsymbol{r}) = c(\boldsymbol{r})\sum_h v_h\exp(i\,\boldsymbol{b}_h\,\boldsymbol{r}), \tag{3}$$

where $\boldsymbol{b}_h$ is a reciprocal lattice vector multiplied by $2\,\pi$ and $c(\boldsymbol{r})$ the shape function, namely,

$$c(\boldsymbol{r}) = 1 \text{ inside the crystal,} \qquad c(\boldsymbol{r}) = 0 \text{ outside the crystal.}$$

For getting BORN's expansion, we put

$$\psi(\boldsymbol{r}) = \psi^{(0)}(\boldsymbol{r}) + \psi^{(1)}(\boldsymbol{r}) + \dots\,. \tag{4}$$

Beginning with

$$\psi^{(0)}(\boldsymbol{r}) = \exp(i\,\boldsymbol{K}_0\,\boldsymbol{r})\,,$$

we obtain by iteration

$$\psi^{(n)}(\boldsymbol{r}) = \left(\frac{2\,m}{\hbar^2}\right)^n\int\cdots\int G(\boldsymbol{r},\boldsymbol{r}_1)\,G(\boldsymbol{r}_1,\boldsymbol{r}_2)\dots G(\boldsymbol{r}_{n-1},\boldsymbol{r}_n)$$
$$\cdot V(\boldsymbol{r}_1)\,V(\boldsymbol{r}_2)\dots V(\boldsymbol{r}_n)\exp(i\,\boldsymbol{K}_0\,\boldsymbol{r}_n)\,\mathrm{d}(\boldsymbol{r}_1)\dots\mathrm{d}(\boldsymbol{r}_n)\,. \tag{5}$$

We choose the coordinate origin inside the crystal and assume that $r \gg r_i$ $(i=1,\ 2,\dots)$. Then we may use, instead of (2), the asymptotic form of GREEN's function, namely,

$$G(\boldsymbol{r},\boldsymbol{r}_1) = -\frac{\exp(i\,K_0\,r)}{4\,\pi\,r}\exp(-i\,\boldsymbol{K}\,\boldsymbol{r}_1), \tag{6}$$

where $\boldsymbol{K}$ is the scattering vector having the length K_0.

Substituting (2), (3) and (6) into (4) and (5), we can rewrite the wave function using a scattering amplitude, $F(\boldsymbol{K},\boldsymbol{K}_0)$, as follows:

$$\psi(\boldsymbol{r}) = \exp(i\,\boldsymbol{K}_0\,\boldsymbol{r}) + \frac{\exp(i\,K_0\,r)}{r}F(\boldsymbol{K},\boldsymbol{K}_0),\quad F(\boldsymbol{K},\boldsymbol{K}_0) = \sum_h F_h(\boldsymbol{K},\boldsymbol{K}_0) = \sum_h\sum_n F_h^{(n)}(\boldsymbol{K},\boldsymbol{K}_0), \tag{7}$$

where $F_h(\boldsymbol{K},\boldsymbol{K}_0)$ is the scattering amplitude for the h-reflection and $F_h{}^{(n)}(\boldsymbol{K},\boldsymbol{K}_0)$ is given by

$$F_h{}^{(n)}(\boldsymbol{K},\boldsymbol{K}_0) = \frac{(-1)^{n-1}\,2\,\pi^2}{(2\,\pi)^{3n}}\sum_{g_1,g_2,\dots,g_{n-1}} v_{h-g_1}\,v_{g_1-g_2}\cdots v_{g_{n-1}}$$
$$\cdot\int\cdots\int\frac{\exp[i(\boldsymbol{k}_{n-1}-\boldsymbol{K}+\boldsymbol{b}_{h-g_1})\,\boldsymbol{r}_1]\exp[i(\boldsymbol{k}_{n-2}-\boldsymbol{k}_{n-1}+\boldsymbol{b}_{g_1-g_2})\,\boldsymbol{r}_2]\dots\exp[i(\boldsymbol{K}_0-\boldsymbol{k}_1+\boldsymbol{b}_{g_{n-1}})\,\boldsymbol{r}_n]}{(K_0{}^2-k_{n-1}^2+i\,\varepsilon_{n-1})\,(K_0{}^2-k_{n-2}^2+i\,\varepsilon_{n-2})\dots(K_0{}^2-k_1{}^2+i\,\varepsilon_1)} \tag{8}$$
$$\cdot c(\boldsymbol{r}_1)\,c(\boldsymbol{r}_2)\dots c(\boldsymbol{r}_n)\,\mathrm{d}(\boldsymbol{r}_1)\dots\mathrm{d}(\boldsymbol{r}_n)\cdot\mathrm{d}(\boldsymbol{k}_1)\dots\mathrm{d}(\boldsymbol{k}_{n-1})\,.$$

The integrations over $\boldsymbol{r}_1$, $\boldsymbol{r}_2,\dots$ in (8) produce the diffraction functions of $c(\boldsymbol{r}_1)$, $c(\boldsymbol{r}_2),\dots,$ respectively. If the crystal is not too small, the product of these diffraction functions has a large value only if simultaneously the following relations are nearly satisfied:

$$\boldsymbol{k}_1 = \boldsymbol{K}_0 + \boldsymbol{b}_{g_{n-1}} \equiv \boldsymbol{K}_{g_{n-1}},\qquad \boldsymbol{k}_2 = \boldsymbol{K}_0 + \boldsymbol{b}_{g_{n-2}} \equiv \boldsymbol{K}_{g_{n-2}},\quad\dots,\quad\text{and}\quad \boldsymbol{K} = \boldsymbol{K}_0 + \boldsymbol{b}_h \equiv \boldsymbol{K}_h\,.$$

If we separate the integral over $\boldsymbol{k}_i$ into the radial part and surface part, the latter can be approximated by a surface integral over the plane perpendicular to $\boldsymbol{K}_{g_{n-i}}$, because the curvature of the EWALD sphere is very small. Therefore, it is easily seen from Fig. 1 that we can write

$$\boldsymbol{k}_i - \boldsymbol{K}_{g_{n-i}} \cong [(k_i - K_{g_{n-i}})/K_{g_{n-i}}]\,\boldsymbol{K}_{g_{n-i}} + \boldsymbol{\varkappa}_i\,. \tag{9}$$

Substituting (9) into (8) and integrating over $\boldsymbol{\varkappa}_i$, we get

$$F_h^{(n)}(\mathbf{K}, \mathbf{K}_0) = \frac{(-1)^{n-1}}{2(2\pi)^n} \sum_{g_1, g_2, \ldots, g_{n-1}} v_{h-g_1} v_{g_1-g_2} \cdots v_{g_{n-1}}$$

$$\cdot \int \cdots \int \exp(-i\,\boldsymbol{\chi}_h \boldsymbol{r}_1) \frac{\exp[-i\,\mathbf{K}_{g_1}(\boldsymbol{r}_1-\boldsymbol{r}_2)] \exp[i(k_{n-1}/K_{g_1})\,\mathbf{K}_{g_1}(\boldsymbol{r}_1-\boldsymbol{r}_2)]\cdots}{(K_0^2-k_{n-1}^2+i\,\varepsilon_{n-1})\cdots}$$

$$\frac{\cdots \exp[-i\,\mathbf{K}_{g_{n-1}}(\boldsymbol{r}_{n-1}-\boldsymbol{r}_n)] \exp[i(k_1/K_{g_{n-1}})\,\mathbf{K}_{g_{n-1}}(\boldsymbol{r}_{n-1}-\boldsymbol{r}_n)]}{\cdots (K_0^2-k_1^2+i\,\varepsilon_1)} \tag{10}$$

$$\cdot\, \delta(\boldsymbol{r}_1^{(1)}-\boldsymbol{r}_2^{(1)}) \ldots \delta(\boldsymbol{r}_{n-1}^{(n-1)}-\boldsymbol{r}_n^{(n-1)})\, c(\boldsymbol{r}_1) \ldots c(\boldsymbol{r}_n)\, \mathrm{d}(\boldsymbol{r}_1) \ldots \mathrm{d}(\boldsymbol{r}_n)\, \mathrm{d}k_1 \ldots \mathrm{d}k_{n-1},$$

where $\boldsymbol{r}_i^{(j)}$ in the δ-functions is the projection of the vector $\boldsymbol{r}_i$ on the plane perpendicular to $\mathbf{K}_{g_j}$. $\boldsymbol{\chi}_h$ is given by

$$\mathbf{K} = \mathbf{K}_h + \boldsymbol{\chi}_h. \tag{11}$$

We call $\boldsymbol{\chi}_h$ the "vectorial excitation error" (Fig. 2). The δ-functions in (10) indicate that in the integrations $\boldsymbol{r}_i - \boldsymbol{r}_{i+1}$ is to be taken parallel to $\mathbf{K}_{g_i}$.

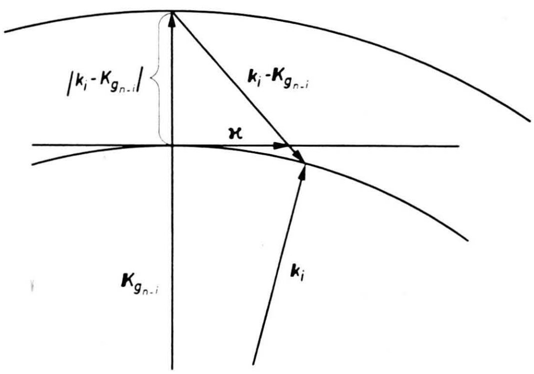

Fig. 1.

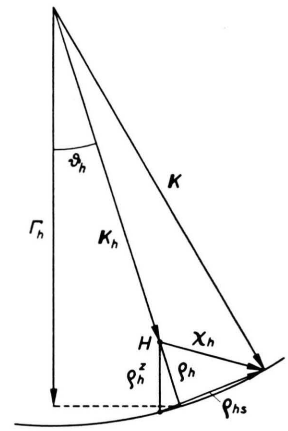

Fig. 2.

The integrals over k_i in (10) are to be evaluated by contour integration on the complex k_i-plane. For $\mathbf{K}_{g_{n-i}} \cdot (\boldsymbol{r}_{n-i} - \boldsymbol{r}_{n+1-i}) > 0$, we have to take the contour on the upper k_i-plane, and for $\mathbf{K}_{g_{n-i}} \cdot (\boldsymbol{r}_{n-i} - \boldsymbol{r}_{n+1-i}) < 0$, on the lower k_i-plane. The former represents a forward scattered and the latter a backward scattered wave. As the backward scattering is generally small, we may neglect the corresponding parts of the integrations.

Putting $\boldsymbol{s}_{g_i} = \mathbf{K}_{g_i}/K_{g_i}$ and adopting the "scalar excitation error" (see Fig. 2)

$$\varrho_{g_i} = K_0 - K_{g_i}, \qquad \text{we obtain} \tag{12}$$

$$F_h^{(n)}(\mathbf{K}, \mathbf{K}_0) = \frac{1}{4\pi}\left(\frac{i}{2K_0}\right)^{n-1} \sum_{g_1, g_2, \ldots, g_{n-1}} v_{h-g_1} v_{g_1-g_2} \ldots v_{g_{n-1}} \cdot \int \cdots \int \exp(-i\,\boldsymbol{\chi}_h \boldsymbol{r}_1) \exp[i\,\varrho_{g_1} \boldsymbol{s}_{g_1}(\boldsymbol{r}_1 - \boldsymbol{r}_2)]$$

$$\ldots \cdot \exp[i\,\varrho_{g_{n-1}} \boldsymbol{s}_{g_{n-1}}(\boldsymbol{r}_{n-1} - \boldsymbol{r}_n)]\, \delta(\boldsymbol{r}_1^{(1)} - \boldsymbol{r}_2^{(1)}) \ldots \delta(\boldsymbol{r}_{n-1}^{(n-1)} - \boldsymbol{r}_n^{(n)}) \cdot c(\boldsymbol{r}_1) \ldots c(\boldsymbol{r}_n)\, \mathrm{d}(\boldsymbol{r}_1) \ldots \mathrm{d}(\boldsymbol{r}_n). \tag{13}$$

The repeated integrations are to be performed under the conditions

$$\boldsymbol{s}_{g_i} \cdot (\boldsymbol{r}_i - \boldsymbol{r}_{i+1}) \geqq 0, \qquad i = 1, 2, \ldots, (n-1). \tag{13 a}$$

§ 2. General Formulae

Fengler applied (13) to a spherical and a parallel-sided crystal and discussed his results only up to the second order Born-approximation. In this section we consider the complete scattering amplitude (7) and try to obtain an approximative evaluation of the integrals in (13) for an arbitrary crystal shape.

Let us consider the integration over $\boldsymbol{r}_n$ in (13). We choose the z_n-axis arbitrarily, the angle between this axis and the vector $\boldsymbol{s}_{g_{n-1}}$ being $\vartheta_{g_{n-1}}$, the x_n- and y_n-axis parallel and perpendicular respectively to the common plane of $\boldsymbol{s}_{g_{n-1}}$ and the z_n-axis. On the other hand we introduce, instead of x_n, a new oblique ξ_n-axis defined by $\xi_n = \cos\vartheta_{g_{n-1}} \cdot x_n - \sin\vartheta_{g_{n-1}} \cdot z_n$, perpendicular to $\boldsymbol{s}_{g_{n-1}}$. Then we have

$$\mathrm{d}(\boldsymbol{r}_n) = \mathrm{d}x_n\,\mathrm{d}y_n\,\mathrm{d}z_n = \frac{\mathrm{d}\xi_n\,\mathrm{d}y_n\,\mathrm{d}z_n}{\cos\vartheta_{g_{n-1}}} = \frac{\mathrm{d}(\boldsymbol{r}_n^{(n-1)})\,\mathrm{d}z_n}{\cos\vartheta_{g_{n-1}}},$$

where $\mathrm{d}(\boldsymbol{r}_n{}^{(n-1)})$ is the element of area normal to $\boldsymbol{s}_{g_{n-1}}$. The vector $\boldsymbol{r}_n$ may be split into the following two components:

$$\boldsymbol{r}_n = \boldsymbol{r}_n{}^{(n-1)} + \left(\xi_n \tan\vartheta_{g_{n-1}} + \frac{z_n}{\cos\vartheta_{g_{n-1}}}\right)\boldsymbol{s}_{g_{n-1}}.$$

Integrating over $\boldsymbol{r}_n{}^{(n-1)}$ (i.e. over $\mathrm{d}\xi_n\,\mathrm{d}y_n$) in (13), we obtain

$$\frac{i}{2K_0}\iiint \exp[i\varrho_{g_{n-1}}\boldsymbol{s}_{g_{n-1}}(\boldsymbol{r}_{n-1}-\boldsymbol{r}_n)]\,\delta(\boldsymbol{r}_{n-1}^{(n-1)}-\boldsymbol{r}_n^{(n-1)})\,c(\boldsymbol{r}_n)\,\mathrm{d}(\boldsymbol{r}_n)$$

$$= \frac{i}{2\Gamma_{g_{n-1}}}\int \exp[i\varrho_{g_{n-1}}^{z}(z_{n-1}-z_n)]\,c(\boldsymbol{r}_{n-1}-\zeta_{g_{n-1}}\boldsymbol{s}_{g_{n-1}})\,\mathrm{d}z_n,$$

with the following abbreviations (cf. Fig. 2):

$$\Gamma_{g_i} = K_0\cos\vartheta_{g_i}, \qquad \varrho_{g_i}^{z} = \varrho_{g_i}/\cos\vartheta_{g_i} = (K_0 - K_{g_i})/\cos\vartheta_{g_i}, \qquad \zeta_{g_i} = (z_i - z_{i+1})/\cos\vartheta_{g_i}. \tag{14}$$

We integrate now over $\boldsymbol{r}_{n-1}^{(n-2)}, \boldsymbol{r}_{n-2}^{(n-3)}, \ldots, \boldsymbol{r}_3^{(2)}, \boldsymbol{r}_2^{(1)}$ with the same procedure, using a common z_i-axis, and obtain

$$\begin{aligned} F_h^{(n)}(\mathbf{K},\mathbf{K}_0) = {} & \frac{K_0}{2\pi i}\left(\frac{i}{2}\right)^n \sum_{g_1,g_2,\ldots,g_{n-1}} \frac{v_{h-g_1}}{\Gamma_h}\frac{v_{g_1-g_2}}{\Gamma_{g_1}}\cdots\frac{v_{g_{n-1}}}{\Gamma_{g_{n-1}}} \\ & \cdot\iint \exp[-i\boldsymbol{\rho}_{hs}\cdot\boldsymbol{r}_1{}^{(h)}]\int\cdots\int \exp[-i(\varrho_h^z-\varrho_{g_1}^z)\,z_1]\ldots\exp[-i(\varrho_{g_{n-2}}^z-\varrho_{g_{n-1}}^z)\,z_{n-1}] \\ & \cdot\exp[-i\varrho_{g_{n-1}}^z z_n]\,c(\boldsymbol{r}_1)\,c(\boldsymbol{r}_1-\zeta_{g_1}\boldsymbol{s}_{g_1})\ldots c(\boldsymbol{r}_1-\sum_{\nu=1}^{n-1}\zeta_{g_\nu}\boldsymbol{s}_{g_\nu})\cdot\mathrm{d}z_n\ldots\mathrm{d}z_1\,\mathrm{d}(\boldsymbol{r}_1{}^{(h)}). \end{aligned} \tag{15}$$

The meaning of $\boldsymbol{\rho}_{hs}$ is shown in Fig. 2: $\quad \boldsymbol{\rho}_{hs} = \boldsymbol{\chi}_h - \varrho_h^z\,\boldsymbol{z}^0, \qquad (16)$

where $\boldsymbol{z}^0$ is the unit vector of the z-direction. $\boldsymbol{r}_1{}^{(h)}$ is the projection of the vector $\boldsymbol{r}_1$ on the plane perpendicular to $\boldsymbol{K}_h$.

We assume that it is possible to regard some part of the crystal surface as the entrance-surface, the remaining part as the exit-surface for the transmitted electrons (LAUE-case). We consider some point P_a on the exit-surface, with the coordinates $\boldsymbol{r}_1{}^{(h)}$, z_a (cf. Fig. 3). For each term of the summation in (15) the z-axis may be chosen in such a way that $\vartheta_{g_i} < \pi/2$ for all g_i. The conditions (13 a) may now be written $\zeta_{g_i} \geqq 0$ for all g_i, or, in other words: $z_1 \geqq z_2 \geqq \ldots \geqq z_n$. A zig-zag-line connecting the points given by the arguments of the shape functions in (15) can be interpreted as a special process of multiple scattering. For a given set of indices $h, g_1, \ldots, g_{n-1}$ all corresponding zig-zag-lines are going through a conical region of the crystal with vertex at P_a, cutting a surface element $P_e{}^1 P_e{}^2$ out of the entrance-surface.

It can easily be seen that the argument of the m-th shape-function, namely the vector $\boldsymbol{r}_1 - \sum_{\nu=1}^{m-1}\zeta_{g_\nu}\boldsymbol{s}_{g_\nu}$, has the component z_m in the z-direction. [In each of the integrations, therefore, the shape-function defining the limits of integration is shifted by some amount perpendicular to the z-axis with respect to the shape-functions of the other integrations.] If the entrance surface element $P_e{}^1 P_e{}^2$ for a definite exit point P_a would be a plane perpendicular to the z-axis, it would be possible to drop the functions $c(\boldsymbol{r}_1-\zeta_{g_1}\boldsymbol{s}_{g_1})\ldots c(\boldsymbol{r}_1-\sum_{\nu=1}^{n-1}\zeta_{g_\nu}\boldsymbol{s}_{g_\nu})$ in the integrand and to write the multiple-integral in the form

$$\int_{z_e}^{z_a}\int_{z_e}^{z_1}\cdots\int_{z_e}^{z_{n-1}}\ldots\,\mathrm{d}z_n\ldots\mathrm{d}z_2\,\mathrm{d}z_1,$$

where z_e and z_a are the z-coordinates of the $P_e{}^1 P_e{}^2$-plane and P_a respectively.

We assume now that the actual crystal shape is such that the normals of the crystal faces are not too much inclined with respect to the z-axis. It will be, then, a reasonable approximative procedure to neglect the effect of the convolution with the laterally shifted shape-functions at all, and to write

$$F_h^{(n)}(\mathbf{K},\mathbf{K}_0) = \frac{K_0}{2\pi i}\left(\frac{i}{2}\right)^n \sum_{g_1, g_2, \dots, g_{n-1}} \frac{v_{h-g_1}}{\Gamma_h} \cdots \frac{v_{g_{n-1}}}{\Gamma_{g_{n-1}}}$$
$$\cdot \iint \exp[-i\,\boldsymbol{\rho}_{hs}\cdot\boldsymbol{r}^{(h)}] \int_{z_e(\boldsymbol{r}^{(h)})}^{z_a(\boldsymbol{r}^{(h)})} \exp[-i(\varrho_h^z - \varrho_{g_1}^z)\,z_1] \int_{z_e(\boldsymbol{r}^{(h)})}^{z_1} \exp[-i(\varrho_{g_1}^z - \varrho_{g_2}^z)\,z_2] \int_{z_e(\boldsymbol{r}^{(h)})}^{z_2} \cdots \tag{17}$$
$$\cdot \int_{z_e(\boldsymbol{r}^{(h)})}^{z_{n-2}} \exp[-i(\varrho_{g_{n-2}}^z - \varrho_{g_{n-1}}^z)\,z_{n-1}] \int_{z_e(\boldsymbol{r}^{(h)})}^{z_{n-1}} \exp[-i\,\varrho_{g_{n-1}}^z\,z_n]\cdot \mathrm{d}z_n\,\mathrm{d}z_{n-1}\dots\mathrm{d}z_2\,\mathrm{d}z_1\,\mathrm{d}(\boldsymbol{r}^{(h)})\,.$$

Here $z_a = z_a(\boldsymbol{r}^{(h)})$ is to be understood as the equation of the exit-surface and z_e is the z-coordinate of some point P_e of the entrance-surface attributed to the point $(\boldsymbol{r}^{(h)}, z_a)$ of the exit-surface (cf. Fig. 3) [2a].

For the complete scattering amplitude $F_h = \sum_{n=1}^{\infty} F_h^{(n)}$, one obtains

$$F_h(\mathbf{K},\mathbf{K}_0) = \frac{K_0}{2\pi i}\iint \exp[-i\,\boldsymbol{\rho}_{hs}\,\boldsymbol{r}^{(h)}]\;\Psi_h(z_e(\boldsymbol{r}^{(h)}),\;z_a(\boldsymbol{r}^{(h)}))\,\mathrm{d}(\boldsymbol{r}^{(h)})\,, \tag{18}$$

where
$$\Psi_h(z_e, z_a) = \{\Omega_{z_e}^{z_a}(\boldsymbol{M})\}_{h0} \tag{19}$$

is the $h0$-element of the "Ω-matrix" [3]

$$\Omega_{z_e}^{z_a}(\boldsymbol{M}) = \boldsymbol{I} + \int_{z_e}^{z_a}\boldsymbol{M}(z_1)\,\mathrm{d}z_1 + \int_{z_e}^{z_a}\boldsymbol{M}(z_1)\int_{z_e}^{z_1}\boldsymbol{M}(z_2)\,\mathrm{d}z_2\,\mathrm{d}z_1 + \dots + \int_{z_e}^{z_a}\boldsymbol{M}(z_1)\int_{z_e}^{z_1}\cdots\int_{z_e}^{z_{n-1}}\boldsymbol{M}(z_n)\,\mathrm{d}z_n\dots\mathrm{d}z_1 + \dots$$

and $\boldsymbol{M}$ is a matrix with the elements

$$M_{g_j\,g_k} = \tfrac{1}{2}\,i(v_{g_j - g_k}/\Gamma_{g_j})\exp[-i(\varrho_{g_j}^z - \varrho_{g_k}^z)\,z]\,.$$

FUJIWARA [4] and the present author [5] have given an evaluation of the multiple integral appearing in (17)

$$(i)^n\int_{z_e}^{z_a}\exp[-i(\varrho_{g_0}^z - \varrho_{g_1}^z)\,z_1]\int_{z_e}^{z_1}\dots\int_{z_e}^{z_{n-1}}\exp[-i\,\varrho_{g_{n-1}}^z\,z_n]\,\mathrm{d}z_n\dots\mathrm{d}z_1$$
$$= \exp[-i\,\varrho_{g_0}^z\,z_a]\sum_{\nu=0}^{n-1}\frac{\exp[i\,\varrho_{g_\nu}^z D]-1}{\varrho_{g_\nu}^z}\prod_{\substack{\mu=0\\(\mu\neq\nu)}}^{n-1}(\varrho_{g_\nu}^z - \varrho_{g_\mu}^z)^{-1}, \tag{20}$$

where we have written g_0 instead of h for convenience, and $z_a - z_e = D$.

The present theory (as FENGLER's) is, however, different from the mentioned theories in the following points: $\mathbf{K}_0$ is not the wave vector in the crystal with the mean inner potential V_0, but in the vacuum, and ϱ_g^z is defined by the EWALD-construction using the wave vectors in the vacuum. The summation over $g_1, \dots, g_{n-1}$ in (17) includes therefore the terms with $g_1 = h$, $g_2 = g_1, \dots, g_{n-1} = 0$ which contain the mean potential v_0. An "addition-theorem" in the theory of the Ω-matrix [3] gives the possibility to get rid of these terms. As shown in the Appendix, we obtain, instead of equation (17),

[2a] z_e is an average z-coordinate of the points of the element $P_e^1\,P_e^2$ of the entrance surface. z_e will be fairly well defined if this surface element is assumed to be small. This assumption will be justified if only scattering through very small angles gives important contributions in the expansion (15). This is equivalent to the so-called column-approximation.

[3] F. R. GANTMACHER, Matrizenrechnung, Deutscher Verlag der Wissenschaften, Berlin 1959, Vol. II, p. 110.

[4] K. FUJIWARA, J. Phys. Soc. Japan **14**, 1513 [1959].

[5] F. FUJIMOTO, J. Phys. Soc. Japan **14**, 1558 [1959]; **15**, 859 [1960].

$$f_h^{(n)}(\mathbf{K}, \mathbf{K}_0) = \frac{K_0}{2\pi i}\left(\frac{i}{2}\right)^n \sum_{g_1,\ldots,g_{n-1}}' \frac{v_{h-g_1}}{\Gamma_h} \cdots \frac{v_{g_{n-1}}}{\Gamma_{g_{n-1}}}$$

$$\cdot \iint \exp[-i\, \boldsymbol{\rho}_{hs}\, \mathbf{r}^{(h)}] \exp\left[i\frac{v_0}{2}\left(\frac{z_a(\mathbf{r}^{(h)})}{\Gamma_h} - \frac{z_e(\mathbf{r}^{(h)})}{\Gamma_0}\right)\right] \tag{21}$$

$$\cdot \int_{z_e(\mathbf{r}^{(h)})}^{z_a(\mathbf{r}^{(h)})} \exp[-i(p_h - p_{g_1})\, z_1] \int_{z_e(\mathbf{r}^{(h)})}^{z_1} \cdots \int_{z_e(\mathbf{r}^{(h)})}^{z_{n-1}} \exp[-i\, p_{g_{n-1}} z_n] \cdot dz_n \ldots dz_1\, d(\mathbf{r}^{(h)})$$

and
$$F_h(\mathbf{K}, \mathbf{K}_0) = \sum_n f_h^{(n)}(\mathbf{K}, \mathbf{K}_0),$$

where p_{g_j} is a redefined excitation-error by the EWALD-construction using the wave vectors in the crystal room of mean inner potential v_0.

$$p_{g_j} = \varrho_{g_j}^z + \tfrac{1}{2} v_0 (1/\Gamma_{g_j} - 1/\Gamma_0). \tag{22}$$

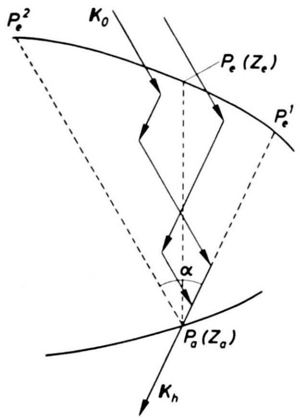

Fig. 3.

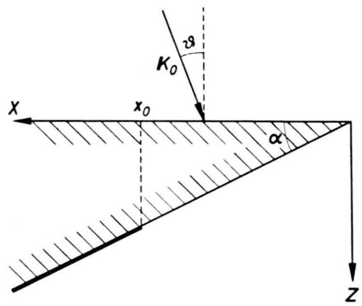

Fig. 4.

The prime at the summation symbol indicates that all terms containing v_0 are to be left out. (19) is also to be rewritten as

$$\Psi_h(z_e, z_a) = \exp\left[i\frac{v_0}{2}\left(\frac{z_a}{\Gamma_h} - \frac{z_e}{\Gamma_0}\right)\right] \psi_h(z_e, z_a), \tag{23}$$

where
$$\psi_h(z_e, z_a) = \{\Omega_{z_e}^{z_a}(\hat{\boldsymbol{M}})\}_{h0} \tag{24}$$

and $\hat{\boldsymbol{M}}$ is the matrix with elements

$$\hat{M}_{g_j g_k} = \tfrac{1}{2} i (v_{g_j - g_k}/\Gamma_{g_j}) \exp[-i(p_{g_j} - p_{g_k})\, z]\ (1 - \delta_{g_j g_k}).$$

The exponential factor in (23) represents the phase shift caused by the difference between the wave vectors in the vacuum and in the crystal. (24) is the BORN-series factor appearing in the theory of scattering from a parallel sided crystal [4, 5] and the Ω-matrix is the same as the scattering matrix obtained by the present author [5]. In that case the transmitted wave of the h-reflection has the well-known form

$$u_h(\mathbf{r}) = \psi_h(z_e, z_a) \exp\left[i\frac{v_0}{2}\left(\frac{z_a}{\Gamma_h} - \frac{z_e}{\Gamma_0}\right)\right] \exp[i(\mathbf{K}_h + \varrho_h^z\, \mathbf{z}^0)\, \mathbf{r}].$$

(18) gives the scattering amplitude from a crystal with arbitrary shape under the assumption that the normal of the entrance surface is not too much inclined to the z-axis. In the case of high electron energy we can frequently assume that $\vartheta_h \cong \vartheta_{g_1} \cong \ldots \cong \vartheta_{g_{n-1}} \cong \vartheta_0$ approximately. p_{g_i} is in this case

equal to ϱ_{gi}^{z} and we obtain, instead of (17),

$$F_h^{(n)}(\mathbf{K},\mathbf{K}_0)=\frac{K_0}{2\pi i}\iint\sum_{g_1,g_2,\ldots,g_{n-1}}\frac{v_{h-g_1}v_{g_1-g_2}\cdots v_{g_{n-1}}}{2^n K_0^n}\exp(-i\boldsymbol{\chi}_h\mathbf{r}_a)\cdot\sum_{\nu=0}^{n-1}\frac{\exp(i\varrho_{g_\nu}D_0)-1}{\varrho_{g_\nu}}\prod_{\substack{\mu=0\\(\mu\neq\nu)}}^{n-1}(\varrho_{g_\nu}-\varrho_{g_\mu})^{-1}\,\mathrm{d}(\mathbf{r}_a^{(h)}),\tag{25}$$

using the relations (14), (20) and $\boldsymbol{\chi}_h\mathbf{r}_a=\varrho_h^z z_a+\boldsymbol{\rho}_{hs}\mathbf{r}_a^{(h)}$, and putting $h=g_0$ in the summation. Here $D_0=(z_a-z_e)/\cos\vartheta_0$ means the path length of the electron in the crystal and is independent of the selection of the z-axis as well as the other quantities. (25), and consequently (18), is therefore approximately valid for an arbitrarily chosen coordinate system. This fact can be understood from the situation that the surface element $P_e^1 P_e^2$ in Fig. 3 is infinitely small and, therefore, z_e is definitely determined. In this case (18) agrees with the formula obtained by KATO [1]. We shall discuss the applicability of (18) more precisely in a later section.

In the following sections we shall make use of (18) with another interpretation of $\psi_h(z_e,z_a)$. Namely, we shall identify (24) with the h-reflection amplitude from a parallel sided crystal, calculated by the dynamical two-wave approximation. We can verify easily by the usual procedure [6] that in this approximation

$$\psi_h(z_e,z_a)=i\sqrt{\frac{\Gamma_0}{\Gamma_h}}\frac{a_h}{\sqrt{p_h^2+|a_h|^2}}\sin\left[\frac{z_a-z_e}{2}\sqrt{p_h^2+|a_h|^2}\right]\cdot\exp\left[i\frac{z_a-z_e}{2}p_h\right]\exp[-i\,p_h z_a]\tag{26}$$

with the abbreviation $a_h=v_h/\sqrt{\Gamma_0\Gamma_h}$.

§ 3. Wedge-Shaped Crystal

In order to compare the present theory with the usual dynamical theory, we apply (18) to a wedge-shaped crystal. For simplicity, we consider the case where the primary beam is perpendicular to the edge of the crystal and we put $\Gamma_h\cong\Gamma_0=K_0\cdot\cos\vartheta_0$ and consequently $p_h\cong\varrho_h^z$ approximately. The geometrical conditions are shown in Fig. 4.

We choose the z-axis parallel to the normal of the entrance surface, the x- and y-axes on the entrance surface along the crystal edge and perpendicular to it, respectively. If we substitute (26) into (18), we obtain

$$F_h(\mathbf{K},\mathbf{K}_0)=\frac{K_0}{2\pi}\frac{a_h}{\sqrt{(\varrho_h^z)^2+|a_h|^2}}\cdot\int_{-y_0}^{y_0}\int_0^{x_0}\sin(p\,x)\exp(i\,q\,x)\exp(-i\,\varrho_{h\eta}\,y)\,\frac{\cos(\alpha-\vartheta)}{\cos\alpha}\,\mathrm{d}x\,\mathrm{d}y\tag{27}$$

with

$$p=\tfrac{1}{2}\tan\alpha\sqrt{(\varrho_h^z)^2+|a_h|^2},\quad q=-\varrho_{h\xi}\frac{\cos(\alpha-\vartheta)}{\cos\alpha}-\frac{1}{2}\tan\alpha\left(\varrho_h^z-\frac{v_0}{\Gamma_0}\right),\tag{28}$$

where α is the angle of the wedge and $\varrho_{h\xi}$ and $\varrho_{h\eta}$ are the components of $\boldsymbol{\rho}_{hs}$ normal and parallel to the crystal edge, respectively. x_0 and y_0 are the coordinates of the contours of an aperture placed on the exit surface. After the integration we obtain the following expression for the intensity:

$$I_h=|F_h(\mathbf{K},\mathbf{K}_0)|^2\Big/\left[2\,x_0\,y_0\frac{\cos(\alpha-\vartheta)}{\cos\alpha}\right]=\frac{K_0^2}{2\pi^2}\frac{|a_h|^2}{(\varrho_h^z)^2+|a_h|^2}\frac{\cos(\alpha-\vartheta)}{\cos\alpha}\frac{1}{(p^2-q^2)\,x_0}\cdot\left[-\sin^2(p\,x_0)+\frac{2p}{p+q}\sin^2\left(\frac{p+q}{2}x_0\right)+\frac{2p}{p-q}\sin^2\left(\frac{p-q}{2}x_0\right)\right]\frac{\sin^2(\varrho_{h\eta}\,y_0)}{(\varrho_{h\eta})^2\,y_0},\tag{29}$$

$I_h\,\mathrm{d}\omega$ represents the probability of scattering of one electron into the solid-angle-element $\mathrm{d}\omega$. If we consider the limiting case $x_0,\ y_0\to\infty$, we get

$$I_h=\frac{K_0^2|a_h|^2}{(\varrho_h^z)^2+|a_h|^2}\frac{\cos(\alpha-\vartheta)}{2\cos\alpha}\frac{1}{4}\left[\delta\left(\frac{p+q}{2}\right)+\delta\left(\frac{p-q}{2}\right)\right]\delta(\varrho_{h\eta}),\tag{30}$$

since the first term in the bracket in (29) vanishes.

[6] See, for example, Z. G. PINSKER, Electron Diffraction (Engl. ed. 1953 Butterworth Sci. Publ. London 1953).

(30) shows that the diffraction spot splits into two sharp peaks, the positions of the peaks being represented by $p = \pm q$. When we use (28) and $\varrho_h^z = \varrho_h/\cos\vartheta$ where ϱ_h is the usual scalar resonance error (Fig. 2), the positions of the peaks are given by

$$\varrho_{h\xi} = \frac{1}{2\cos\vartheta}\left\{\frac{v_0}{K_0} - \varrho_h \pm \sqrt{\varrho_h^2 + \frac{|v_h|^2}{K_0^2}}\right\}\frac{\sin\alpha}{\cos(\alpha-\vartheta)}. \tag{31}$$

The first term in (31) represents the refraction effect caused by the mean inner potential and the second term shows the double refraction caused by the existence of two wave fields. The formula is identical with that obtained by the usual dynamical theory [1].

§ 4. Spherical Crystal

a) Scattering Amplitude

In this section we intend to apply (18) to a spherical crystal which is held in a parallel sided polycrystalline foil. If the spherical crystal nearly satisfies the BRAGG condition and the other crystallites do not, we may put $v_0 = 0$.

We choose the z-axis in the direction of the incident beam and the origin of the cylindrical coordinate system (z, r, φ) on the center of the spherical crystal with radius R. z_e and z_a are then given by

$$z_e = -\sqrt{R^2 - r^2}, \qquad z_a = \sqrt{R^2 - r^2}, \tag{32}$$

respectively. We assume again $\vartheta_h \cong \vartheta_0 = 0$ approximately, which means $\varrho_h^z = \varrho_h$ and $a_h = v_h/K_0$.

Substituting (26) and (32) into (18), we obtain

$$F_h(\mathbf{K}, \mathbf{K}_0) = \frac{K_0}{2\pi}\frac{a_h}{\sqrt{\varrho_h^2 + |a_h|^2}} \cdot \int_0^R \int_0^{2\pi} \sin[\sqrt{R^2 - r^2}\sqrt{\varrho_h^2 + |a_h|^2}]\exp(-i\,\varrho_{hs}\, r\cos\varphi)\, r\, d\varphi\, dr, \tag{33}$$

where φ is the angle between $\boldsymbol{\rho}_{hs}$ and $\mathbf{r}_a^{(h)}$. After the integration over φ, we get, substituting $r = R\sin t$,

$$\begin{aligned} F_h(\mathbf{K}, \mathbf{K}_0) &= \frac{K_0\, a_h}{\sqrt{\varrho_h^2 + |a_h|^2}} \int_0^R \sin[\sqrt{R^2 - r^2}\sqrt{\varrho_h^2 + |a_h|^2}]\, J_0(\varrho_{hs}\, r)\, r\, dr \\ &= \frac{R^2 K_0\, a_h}{\sqrt{\varrho_h^2 + |a_h|^2}} \int_0^{\pi/2} \sin[R\sqrt{\varrho_h^2 + |a_h|^2}\cos t] \cdot J_0(R\,\varrho_{hs}\sin t)\cos t\sin t\, dt, \end{aligned} \tag{34}$$

where J_0 is the 0-th order BESSEL function. Using the well-known integral representation of the 1-st order spherical BESSEL function [7], namely,

$$j_1(z) = \frac{1}{\cos\vartheta}\int_0^{\pi/2} \sin(z\cos\vartheta\cos t)\, J_0(z\sin\vartheta\sin t)\,\cos t\sin t\, dt$$

and putting $\qquad z\cos\vartheta = R\sqrt{\varrho_h^2 + |a_h|^2}, \qquad z\sin\vartheta = R\,\varrho_{hs},$

we obtain

$$F_h(\mathbf{K}, \mathbf{K}_0) = \frac{R^2 K_0\, a_h}{\sqrt{\chi_h^2 + |a_h|^2}}\, j_1(R\sqrt{\chi_h^2 + |a_h|^2}). \tag{35}$$

The kinematical value corresponding to (35) is $F_h^{k}(\mathbf{K}, \mathbf{K}_0) = \dfrac{R^2 K_0\, a_h}{|\chi_h|}\, j_1(R\,|\chi_h|)$. (35′)

(35) shows that the intensity distribution in the dynamical scattering theory has a spherical symmetry as in the kinematical case.

[7] P. M. MORSE and H. FESHBACH, Methods of Theoretical Physics, McGraw-Hill, New York 1953, Vol. II, p. 1575.

b) Line Profile of a Debye–Scherrer Ring

When we choose the rectangular coordinates as shown in Fig. 5, the line profile of the DEBYE–SCHERRER ring is expressed by

$$I_h(\chi_{hx}) = \iint |F_h|^2 \frac{2\pi b_h}{4\pi b_h^2} d\chi_{hz} \frac{1}{K_0} d\chi_{hy} = \frac{1}{2 b_h K_0} \iint |F_h|^2 d\chi_{hy} d\chi_{hy}, \tag{36}$$

where the subindices in χ_h denote the components of $\boldsymbol{\chi}_h$. The coefficient $2\pi b_h/(4\pi b_h^2)$ is due to the averaging over all crystal orientations. Substituting (35) into (36) and transforming the integral from $y-z$ coordinates to polar coordinates (χ_{hp}, φ), we get

$$\begin{aligned} I_h(\chi_{hx}) &= \frac{R^4 K_0 |a_h|^2}{2 b_h} \int_0^\infty \int_0^{2\pi} \frac{\chi_{hp}}{\chi_{hp}^2 + \chi_{hx}^2 + |a_h|^2} j_1^2(R\sqrt{\chi_{hp}^2 + \chi_{hx}^2 + |a_h|^2})\, d\varphi\, d\chi_{hp} \\ &= \frac{\pi R^4 K_0 |a_h|^2}{b_h} \int_0^\infty \frac{\chi_{hp}}{\chi_{hp}^2 + \chi_{hx}^2 + |a_h|^2} j_1^2(R\sqrt{\chi_{hp}^2 + \chi_{hx}^2 + |a_h|^2})\, d\chi_{hp} \\ &= \frac{\pi R^4 K_0 |a_h|^2}{b_h} \int_{R\sqrt{\chi_{hx}^2 + |a_h|^2}}^\infty \frac{1}{t} j_1^2(t)\, dt. \end{aligned}$$

After the integration, we obtain

$$\begin{aligned} I_h(\chi_{hx}) &= \frac{\pi R^2 K_0 |a_h|^2}{4 b_h} \frac{1}{\chi_{hx}^2 + |a_h|^2} \left[1 - \frac{\sin(2R\sqrt{\chi_{hx}^2 + |a_h|^2})}{R\sqrt{\chi_{hx}^2 + |a_h|^2}} + \frac{\sin^2(R\sqrt{\chi_{hx}^2 + |a_h|^2})}{R^2\sqrt{\chi_{hx}^2 + |a_h|^2}}\right] \\ &= \frac{\pi R^2 K_0 |a_h|^2}{4 b_h} \frac{1}{\chi_{hx}^2 + |a_h|^2} \left[1 + \frac{1}{2R^2(\chi_{hx}^2 + |a_h|^2)} + 2 n_1(2R\sqrt{\chi_{hx}^2 + |a_h|^2})\right], \end{aligned} \tag{37}$$

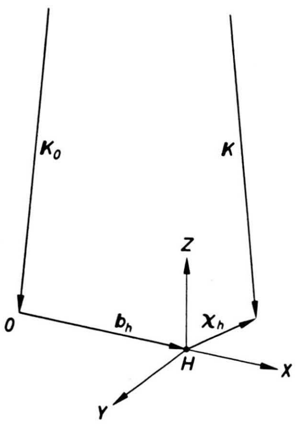

Fig. 5.

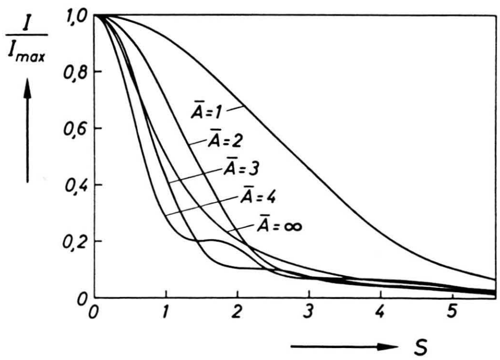

Fig. 6. Line profile of the DEBYE–SCHERRER ring from a spherical crystal. The variables S and A are given by (38) and (45), respectively.

where $\quad n_1(z) = -\frac{\cos z}{z^2} - \frac{\sin z}{z}$

is the 1-st order spherical NEUMANN function.

If we rewrite (37) with the new parameters

$$S = \frac{\chi_{hx}}{|a_h|}, \quad A = 2R|a_h| = D|a_h|, \tag{38}$$

(D: diameter),

(37) becomes

$$I_h(S) = \frac{\pi R^2 K_0}{4 b_h (1+S^2)} \cdot \left[1 + \frac{2}{A^2(1+S^2)} + 2 n_1(A\sqrt{1+S^2})\right]. \tag{39}$$

The corresponding kinematical formula is

$$I_h^{\mathrm{k}}(S) = \frac{\pi R^2 K_0}{4 b_h S^2}\left[1 + \frac{2}{A^2 S^2} + 2 n_1(A S)\right]. \tag{39'}$$

In the limiting case, $A \rightarrow \infty$, (39) becomes

$$I_h(S) \rightarrow \frac{\pi R^2 K_0}{4 b_h (1+S^2)} . \tag{40}$$

(39) and (40) are shown in Fig. 6.

c) Integrated Intensity

The integrated intensity can be expressed by

$$J_h = \frac{1}{K_0} \int I_h \, \mathrm{d}\chi_{hx} . \tag{41}$$

On the other hand, we can rewrite (39) as follows:

$$I_h(S) = \frac{\pi R^2 K_0}{2 b_h} \frac{1}{A} \left[\int_0^A \int_0^{x'} \frac{\sin(x \sqrt{1+S^2})}{\sqrt{1+S^2}} \mathrm{d}x \, \mathrm{d}x' \right. \tag{42}$$

$$\left. - \frac{1}{A} \int_0^A \int_0^{x''} \int_0^{x'} \frac{\sin(x \sqrt{1+S^2})}{\sqrt{1+S^2}} \mathrm{d}x \, \mathrm{d}x' \, \mathrm{d}x'' \right] .$$

Substituting (42) into (41), we obtain [7]

$$J_h = \frac{\pi^2 R}{4 b_h} \left[\int_0^A \int_0^{x'} J_0(x) \, \mathrm{d}x \, \mathrm{d}x' \right. \tag{43}$$

$$\left. - \frac{1}{A} \int_0^A \int_0^{x''} \int_0^{x'} J_0(x) \, \mathrm{d}x \, \mathrm{d}x' \, \mathrm{d}x'' \right] .$$

This formula corresponds to BLACKMAN's formula [8] which was calculated for a parallel sided crystal, namely,

$$J_h^{\mathrm{B}} = \frac{\pi \, | a_h |}{4 b_h} \int_0^{A'} J_0(x) \, \mathrm{d}x \tag{44}$$

where $A' = H \, | a_h |$ and H is the crystal thickness.

In order to compare (43) with (44), we should take the integrated intensity for unit volume of the scatterer and rewrite the formulae in an expanded form. Moreover, it is convenient to use a parameter $\bar{A}$ given by

$$\bar{A} = \bar{D} \, | a_h | \quad (\bar{D} = \sqrt[3]{4 \pi / 3} \, R) , \tag{45}$$

instead of A, where $\bar{D}$ is the mean grain size. The results are as follows:

$$J_h / (4 \pi R^3 / 3) = \frac{\pi \, | a_h |^2}{4 b_h} \left[1 - \frac{1}{20} A^2 + \frac{1}{746.7} A^4 - \dots \right]$$

$$= \frac{\pi \, | a_h |^2}{4 b_h} \left[1 - \frac{1}{12.99} \bar{A}^2 + \frac{1}{315.1} \bar{A}^4 - \dots \right] \tag{46}$$

[8] M. BLACKMAN, Proc. Roy. Soc., Lond. A **173**, 68 [1939].

and

$$J_h^{\mathrm{B}} / H = \frac{\pi \, | a_h |^2}{4 b_h} \left[1 - \frac{1}{12} A'^2 + \frac{1}{320} A'^4 - \dots \right] \tag{47}$$

where the factor

$$J_h^{\mathrm{k}} = \pi \, | a_h |^2 / (4 b_h) \tag{48}$$

is the integrated intensity calculated by the kinematical theory. As we see from (46) and (47), the discrepancy between the integrated intensities obtained from a spherical and a parallel plate crystal is very small in the case of small $\bar{A}$ and A'. These results are shown in Fig. 7.

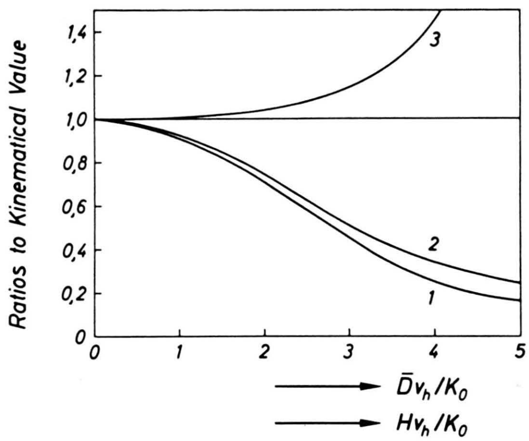

Fig. 7. Ratios of the integrated intensities and line breadths to the corresponding kinematical values. Curve 1: Integrated intensity calculated for a parallel sided crystal (BLACKMAN's curve). Curve 2: Integrated intensity calculated for a spherical crystal. Curve 3: Line breadth of the DEBYE–SCHERRER ring calculated for a spherical crystal. — The abscissa is $H \, v_h / K_0$ for Curve 1 and $\bar{D} \, v_h / K_0$ for Curves 2 and 3.

In the limiting case, A and $A' \rightarrow \infty$, the integrated intensities for unit area of entrance surface become

$$J_h / \pi R^2 \rightarrow \pi \, | a_h | / (4 b_h) ,$$
$$J_h^{\mathrm{B}} \rightarrow \pi \, | a_h | / (4 b_h) . \tag{49}$$

This agreement is reasonable from the physical point of view.

d) Line Breadth of a Debye–Scherrer Ring

The integral line breadth of the DEBYE–SCHERRER ring is given by

$$\beta = J_h / I_h(0) . \tag{50}$$

When we put (39) and (43) into (50), and express (50) in an expanded form, the integral breadth is given by

$$\beta = \frac{4\,\lambda}{3\,D}\left[1 + \frac{1}{180}A^2 + \frac{1}{3860.4}A^4 - \dots\right] \tag{51}$$

where λ is the DE BROGLIE-wave length. Here the factor

$$\beta^{\mathrm{k}} = 4\,\lambda/(3\,D) \tag{52}$$

is the kinematical value of the integral breadth obtained by STOKES and WILSON [9]. (51) indicates that the magnitude $\beta\,D/\lambda$ is not a constant but rather a function of λ, D and v_h. The discrepancy between the kinematical value and the dynamical one is, however, much smaller than in the case of the integrated intensity, as far as A is very small. In the region of large A, we must calculate more accurately. The result is shown in Fig. 7. This result indicates that the integral breadth departs from the kinematical value at some value of A and the difference increases rapidly with A.

In the limiting case, $A \to \infty$, the value $\beta/(|\,v_h\,|/K_0^2)$ becomes

$$\beta/(|\,v_h\,|/K_0^2) \to \pi\,. \tag{53}$$

In Fig. 8, we show the variations of $\beta/(|\,v_h\,|/K_0^2)$ and $\beta^{\mathrm{k}}/(|\,v_h\,|/K_0^2)$.

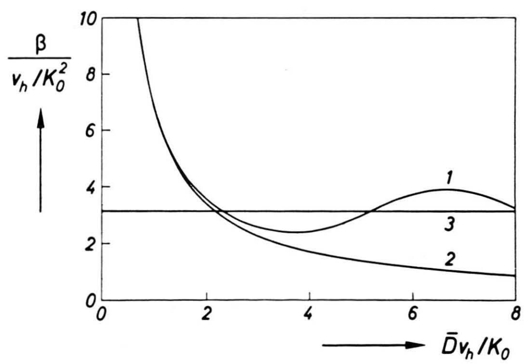

Fig. 8. The line breadth of the DEBYE–SCHERRER ring calculated for a spherical crystal. Curve 1: Curve obtained by the present theory. Curve 2: Kinematical curve. Curve 3: Value of Curve 1 in the limiting case, $D\,v_h/K_0 \to \infty$.

§ 5. Comparison with Experiment

The dynamic effect of the integrated intensity has been recently studied experimentally by many workers. In any case, we cannot say whether the crystallites in the foil have a spherical or parallel sided form. It may be reasonable, however, to consider that a film, which has been very carefully prepared, consists of crystallites of a nearly spherical form. As one of the recent experiments we can cite the study of HORSTMANN and MEYER [10] who investigated the scattering from aluminium. They prepared the foils carefully and measured only elastic scattering. In the following we shall compare their results with our theory.

As we can see in Fig. 7, the difference between the integrated intensity calculated by BLACKMAN's formula and that obtained by the present theory is very small. If we use the grain size D', which is given by the usual SCHERRER formula $\beta = \lambda/D'$, instead of $\bar{D}$, given by (52), both curves agree almost completely. On the other hand, the experimental values show very good agreement with the theoretical ones except the values for higher order reflections, though there is a small difference between the best fitting grain size, D_{dyn}, and the observed one, D_0. When we consider the experimental accuracy, the error of the SCHERRER constant or of the distribution of grain size, it is almost impossible to distinguish experimentally the values of the integrated intensity which are calculated for a parallel sided crystal and for a spherical one. A larger difference can rather be found in the line breadths.

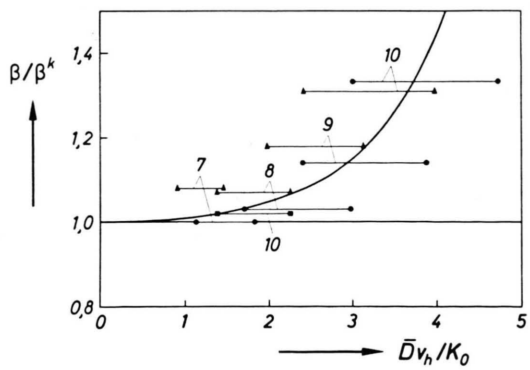

Fig. 9. Experimental values of the line breadth of DEBYE–SCHERRER rings from Al compared with the theoretical curve. Circle: 111-reflection, Triangle: 200-reflection and Rectangle: 220-reflection. Numbers indicate the sample number. Observed grain size of each sample is 260 Å for No. 10, 210 Å for No. 9, 150 Å for No. 8 and 110 Å for No. 7. As experimental values the average values in the range of accelerating voltages between 20 kV and 50 kV have been taken.

[9] A. R. STOKES and A. J. C. WILSON, Proc. Cambridge Phil. Soc. **38**, 313 [1942].

[10] M. HORSTMANN and G. MEYER, Acta Cryst. **15**, 271 [1962]. — A_h in their work is half our A.

As concerns HORSTMANN and MAYER's line breadths[11] their values β/λ as function of $\bar{D}\,v_h$ for most of the reflections lie on a straight line except for the 111- and 200-reflections. The line breadths of the 111- and 200-reflections are larger than the values for the other reflections and the difference increases with the grain size. Though the straight line is not parallel to the abscissa, since there is some strain in the crystallites, we take the straight line as the kinematical value for each reflection. The ratios of the observed values to the kinematical ones for each reflection and each grain size are shown in Fig. 9. The horizontal lines indicate the range of error due to the fact that the observed values are mean values for accelerating voltages from 20 kV to 50 kV.

The results agree well with the theoretical curve. This may indicate that the crystallites in the foil have not the form of parallel sided plates. For the 200-reflection, the line breadth is larger than the kinematical one even in the case of small grain sizes. The reason may be that the crystallites are not completely spherical.

In this section we compared only the first order reflections. In the case of second order reflections, such as 222 and 400, the observed values of the integrated intensity and line breadth are quite different from the theoretical ones obtained from the two-wave-approximation. In this case, we should calculate with the multiple-wave-theory.

§ 6. Discussion

a) As mentioned in § 2, (18) gives a correct expression for the scattering amplitude from a finite crystal under the assumption that the z-axis is normal to the entrance surface or the wave vectors can be assumed to be parallel to each other. In the case where the angles between the wave vectors are not negligibly small and the z-axis is much inclined to the entrance surface, however, (18) is no more correct. We consider now the applicability of (18).

For simplicity, we adopt (26) as $\psi(z_e, z_a)$ and put $v_0 = 0$ as in section 4. In the case where the z-axis is perpendicular to the entrance surface and the scattering angle $\alpha = \vartheta_0 - \vartheta_h$ is small, the scattering amplitude is given by

$$\begin{aligned} F_h(\mathbf{K}, \mathbf{K}_0) &= \frac{K_0}{2\pi i} \iint \exp(-i\,\boldsymbol{\rho}_{hs}\,\boldsymbol{r}_a^{(h)})\,\frac{i}{\Gamma_h}\,\frac{v_h}{\sqrt{(\varrho_h^z)^2 + \dfrac{|v_h|^2}{\Gamma_0\Gamma_h}}} \\ &\quad\cdot \sin\left(\frac{z_a - z_e}{2}\sqrt{(\varrho_h^z)^2 + \frac{|v_h|^2}{\Gamma_0\Gamma_h}}\right) \exp\left(-i\,\varrho_h^z\,\frac{z_a + z_e}{2}\right) \mathrm{d}(\boldsymbol{r}_a^{(h)}) \qquad (54) \\ &\cong \frac{1}{2\pi} \iint \frac{v_h}{\sqrt{\varrho_h^2 + (|v_h|/K_0)^2\,(1 + \alpha\tan\vartheta_h)}} \\ &\quad\cdot \sin\left(\frac{D_h}{2}\sqrt{\varrho_h^2 + (|v_h|/K_0)^2\,(1 + \alpha\tan\vartheta_h)}\right) \exp\left(i\,\varrho_h\,\frac{D_h}{2}\right) \exp(-i\,\boldsymbol{\chi}_h\,\boldsymbol{r}_a) \cdot \mathrm{d}(\boldsymbol{r}_a^{(h)}), \end{aligned}$$

where $D_h = (z_a - z_e)/\cos\vartheta_h$ is independent of the coordinate system. We consider next the case of the z-axis parallel to $\mathbf{K}_h$. The angle between the z-axis and the normal of the entrance surface is ϑ_h and the scattering amplitude is given by

$$F_h(\mathbf{K}, \mathbf{K}_0) = \frac{1}{2\pi} \iint \frac{v_h}{\sqrt{\varrho_h^2 + (|v_h|/K_0)^2}} \sin\left(\frac{D_h}{2}\sqrt{\varrho_h^2 + (|v_h|/K_0)^2}\right) \exp\left(i\,\varrho_h\,\frac{D_h}{2}\right) \exp(-i\,\boldsymbol{\chi}_h\,\boldsymbol{r}_a)\, \mathrm{d}(\boldsymbol{r}_a^{(h)}) \qquad (55)$$

under the same approximation.

As seen easily from (54) and (55), the error caused by the different z-axis is maximum at $\varrho_h = 0$ and is determined by the quantity $\alpha\tan\vartheta_h$ for small $D_h\,v_h/K_0$. If we take $\alpha\tan\vartheta_h = 1/10$ as a critical condition and $\alpha = 1/50$, the critical angle ϑ_h is about 78°. For large $D_h\,v_h/K_0$, the error is determined by the quantity $(D_h\,v_h/4\,K_0)$ $\alpha\tan\vartheta_h$ rather than $\alpha\tan\vartheta_h$. If we take, for example, D_h = 500 Å, K_0 = 100 Å^{-1}, v_h = 2 Å^{-1} and $\alpha = 1/50$ and $(D_h\,v_h/4\,K_0)$ $\alpha\tan\vartheta_h = 1/10$ as a critical condition, the critical angle ϑ_h is about 64°. In actual case, however, D_h may be not so large as in the above example, so long as we consider the scattering from a polycrystalline foil. For a spherical crystal with D = 500 Å, for example, D_h at $\vartheta_h = 78°$ is about 100 Å and $(D_h\,v_h/K_0)\,\alpha\tan\vartheta_h = 1/20$. Furthermore,

[11] See Fig. 8 in their work [10].

the contribution of the region with ϑ_h larger than 78° to the intensity may be small.

From the above consideration, we can conclude that the errors arising from the selection of the z-axis or neglect of the scattering angle are practically very small, though the estimation of errors in a general case is very complicated. The above discussion shows that the present theory is essentially equivalent to the column approximation which corresponds to dividing the crystal into columns parallel to the wave vector.

b) In section 4, a spherical crystal held in a parallel sided foil has been taken into account and the mean potential which causes the refraction effect has been neglected. The result showed an anomaly of the line breadth of a DEBYE–SCHERRER ring. We can say that this anomaly is due to a double refraction based on the two wave fields in the crystal and call this anomaly "dynamic effect of line breadth".

Of course, it is not possible to fill up a parallel sided foil with spherical crystallites and crystallites in a foil cannot have only spherical form. The dynamic effect, however, should also appear when the form and orientation of the crystallites is at random and, if this is the case, the magnitude of the dynamic effect may be of the same order as that obtained from a spherical crystal.

The experiment of HORSTMANN and MEYER has shown good agreement with the theoretical values of this dynamic effect regarding the dependence on crystal size. The dependence on wave length should be studied in future.

I wish to express my sincere thanks to Prof. Dr. H. RAETHER of Hamburg University and Prof. Dr. K. MOLIÈRE of Fritz-Haber-Institut for encouragements and for giving the opportunity to work in their laboratories. — The author thanks Dr. M. HORSTMANN and Dr. G. MEYER of Hamburg University and Dr. K. KAMBE of Fritz-Haber-Institut for helpful discussions.

Appendix

Elimination of the terms containing v_0 from the BORN-*expansion*

It is known [3], that, if

$$\boldsymbol{M}' + \boldsymbol{N} = \boldsymbol{M},$$

it follows that

$$\Omega_{z_e}^{z_a}(\boldsymbol{M}' + \boldsymbol{N}) = \Omega_{z_e}^{z_a}(\boldsymbol{N}) \cdot \Omega_{z_e}^{z_a}(\boldsymbol{Q}), \qquad \text{(A 1)}$$

where
$$\boldsymbol{Q} = [\Omega_{z_e}^{z}(\boldsymbol{N})]^{-1}\, \boldsymbol{M}'\, \Omega_{z_e}^{z}(\boldsymbol{N}). \qquad \text{(A 2)}$$

If $\boldsymbol{N}$ is a constant matrix, then $\Omega(\boldsymbol{N})$ is the exponential matrix

$$\Omega_{z_e}^{z}(\boldsymbol{N}) = \exp[\boldsymbol{N}(z - z_e)]$$

so that

$$\boldsymbol{Q} = \exp[-\boldsymbol{N}(z - z_e)]\, \boldsymbol{M}' \exp[\boldsymbol{N}(z - z_e)], \qquad \text{(A 2')}$$

we identify

$$M'_{g_j g_k} = \frac{i}{2} \frac{v_{gj-gk}}{\Gamma_{gj}} \exp[-i(\varrho_{g_j}^z - \varrho_{g_k}^z)\, z]\,(1 - \delta_{gj\,gk}).$$
$$N_{g_j g_k} = \frac{i}{2} \frac{v_0}{\Gamma_{gj}}\, \delta_{gj\,gk}, \qquad \text{(A 3)}$$

so that

$$\{\exp[\boldsymbol{N}(z - z_e)]\}_{g_j g_k} = \exp\left[\frac{i}{2} \frac{v_0}{\Gamma_{gj}} (z - z_e)\right] \delta_{gj\,gk},$$

and

$$\boldsymbol{Q}_{gj\,gk} = \exp\left[i \frac{v_0}{2} \left(\frac{1}{\Gamma_{gj}} - \frac{1}{\Gamma_{gk}}\right) z_e\right] \frac{i\, v_{gj-gk}}{2\, \Gamma_{gj}} \cdot \exp[-i(p_{gj} - p_{gk})\, z]\,(1 - \delta_{gj\,gk}). \qquad \text{(A 4)}$$

Here

$$p_{gj} = \varrho_{g_j}^z + \frac{v_0}{2}\left(\frac{1}{\Gamma_{gj}} - \frac{1}{\Gamma_0}\right) \qquad \text{(A 5)}$$

is a redefined excitation error, taking acount of the refraction. We have introduced in (A 5) the last term $-v_0/2\,\Gamma_0$ in order to get $p_0 = 0$. We finally obtain

$$\{\Omega_{z_e}^{z_a}(\boldsymbol{M})\}_{hh'} = \exp\left[i \frac{v_0}{2}\left(\frac{z_a}{\Gamma_h} - \frac{z_e}{\Gamma_{h'}}\right)\right] \{\Omega_{z_e}^{z_a}(\hat{\boldsymbol{M}})\}_{hh'} \qquad \text{(A 6)}$$

where $\hat{\boldsymbol{M}}$ is a matrix having only non-diagonal elements:

$$\hat{M}_{gj\,gk}(z) = \frac{i}{2} \frac{v_{gj-gk}}{\Gamma_{gj}} \cdot \exp[-i(p_{gj} - p_{gk})\, z]\,(1 - \delta_{gj\,gk}). \qquad \text{(A 7)}$$